Available online at www.sciencedirect.com
ScienceDirect
European Journal of Pharmaceutics and Biopharmaceutics 68 (2008) 368–379
European Journal of Pharmaceutics and Biopharmaceutics
www.elsevier.com/locate/ejpb

Research paper

# In-silico model of skin penetration based on experimentally determined input parameters. Part II: Mathematical modelling of in-vitro diffusion experiments. Identification of critical input parameters

Arne Naegel [a], Steffi Hansen [b], Dirk Neumann [c], Claus-Michael Lehr [b], Ulrich F. Schaefer [b], Gabriel Wittum [a], Michael Heisig [a,*]

[a] *University of Heidelberg, Simulation in Technology, Heidelberg, Germany*
[b] *Saarland University, Biopharmaceutics and Pharmaceutical Technology, Saarbrücken, Germany*
[c] *Saarland University, Center for Bioinformatics Saar, Saarbrücken, Germany*

Received 2 February 2007; accepted in revised form 31 May 2007
Available online 15 June 2007

**Abstract**

This work describes a framework for in-silico modelling of in-vitro diffusion experiments illustrated in an accompanying paper [S. Hansen, A. Henning, A. Naegel, M. Heisig, G. Wittum, D. Neumann, K.-H. Kostka, J. Zbytovska, C.M. Lehr, U.F. Schaefer, In-silico model of skin penetration based on experimentally determined input parameters. Part I: experimental determination of partition and diffusion coefficients, Eur. J. Pharm. Biopharm. XX (2007) xx–xx]. A mathematical model of drug permeation through stratum corneum (SC) and viable epidermis/dermis is presented. The underlying geometry for the SC is of brick-and-mortar character, meaning that the corneocytes are completely embedded in the lipid phase. The geometry is extended by an additional compartment for the deeper skin layers (DSL). All phases are modelled with homogeneous diffusivity. Lipid-donor and SC–DSL partition coefficients are determined experimentally, while corneocyte–lipid and DSL–lipid partition coefficients are derived consistently with the model. Together with experimentally determined apparent lipid- and DSL-diffusion coefficients, these data serve as direct input for computational modelling of drug transport through the skin. The apparent corneocyte diffusivity is estimated based on an approximation, which uses the apparent SC- and lipid-diffusion coefficients as well as corneocyte–lipid partition coefficients. The quality of the model is evaluated by a comparison of concentration–SC-depth-profiles of the experiment with those of the simulation. Good agreements are obtained, and by an analysis of the underlying model, critical parameters of the models can be identified more easily.


*Keywords:* Skin; Drug diffusion; Concentration–depth-profiles; Mathematical modelling; Numerical simulation

## 1. Introduction

Recently, there has been much interest in mathematical models and numerical methods available to predict dermal absorption in-silico in order to avoid unnecessary and costly in-vitro and in-vivo testing [2,3]. To a great extent, this is due to ethical difficulties resulting in a lack of sufficient amounts of human skin. The use of animal skin is limited by animal healthcare regulations and anatomical difference. Economic and time constraints must be considered as well, especially with respect to increasing legislation in the risk assessment of industrial chemicals [4]. Therefore, mathematical modelling and numerical simulation of drug transport through human skin gain key roles in the investigation of dermal and transdermal drug delivery as well as risk assessment of chemical exposure.

* Corresponding author. Simulation in Technology, University of Heidelberg, INF 368, 69120 Heidelberg, Germany. Tel.: +49 6221 54 8861.
*E-mail address:* michael.heisig@iwr.uni-heidelberg.de (M. Heisig).

0939-6411/$ - see front matter © 2007 Elsevier B.V. All rights reserved.
doi:10.1016/j.ejpb.2007.05.018

Today, most of the pharmacokinetic models are based on one or more compartments describing the skin layers and the vehicle [5–10]. The drug concentration in each of these layers is modelled by an ordinary differential equation, which does not provide information about the drug concentrations in the layers of the stratum corneum (SC) and the deeper skin layers (DSL). Furthermore, the parameters like diffusion coefficients and partition coefficients for these equations are model- and system-dependent allowing no direct input for computational simulation of skin transport.

A further mathematical approach for modelling are diffusion models which consist of partial differential equations describing drug delivery in space and time according to Fick's laws of diffusion [11–24,31,33,34]. These models are based on first principles, such as balance of mass. Resolving the structure, they have the great advantage that the parameters, e.g., diffusion and partition coefficients, are system-independent, allowing a system-independent parameter identification. Therefore, the effects of different parameters like corneocyte permeability, corneocyte alignment, diffusion and partition coefficients on skin transport can be studied in-silico on arbitrary skin geometries.

Recently, due to advances in simulation techniques, diffusion models running on fully resolved two-dimensional or even three-dimensional geometries have become feasible. A great part of these models are so-called "brick-and-mortar" models [19–22,25–33]. The bricks and mortar correspond to the corneocytes and the surrounding intercellular lipid bilayers, respectively. A very good survey of existing "brick-and-mortar" models is given by Wang et al. [33].

It was shown several years ago [31] that including the heterogeneous structure of the SC in the geometry is crucial for the barrier function of the membrane. This two-dimensional diffusion model allows to calculate the time-dependent spatial distribution of drugs in the different skin layers and to illustrate the diffusional pathway in the SC. These illustrations are very similar to photographs of SC visualised using two-photon fluorescence microscopy [35–37].

In this paper, we present an extension of our two-dimensional diffusion model [31] by increasing the number of corneocyte layers to 16 and adding a homogeneous epidermal/dermal compartment. To the best of our knowledge, we are the first to use experimentally determined partition coefficients $K_{\mathrm{lip/don}}$, $K_{\mathrm{SC/don}}$ and $K_{\mathrm{SC/DSL}}$ as well as diffusion coefficients $D_{\mathrm{lip}}$, $D_{\mathrm{SC}}$ and $D_{\mathrm{DSL}}$ as input parameters in a 2D-model to evaluate drug concentration-SC/DSL-depth profiles in-silico. The experimental data are presented in an accompanying paper by Hansen et al. [1]. Experimentally not accessible partition coefficients $K_{\mathrm{cor/lip}}$ and $K_{\mathrm{DSL/lip}}$ as well as diffusion coefficient $D_{\mathrm{cor}}$ have been determined as implicit parameters. The data have been successfully modelled by assuming constant partition and diffusion coefficients. As model drugs one lipophilic, however ionisable, substance (flufenamic acid, FFA) and one hydrophilic non-ionisable compound (caffeine) are used. A comparison of the concentration-SC/DSL-depth profiles obtained by in-vitro and in-silico experiments is presented and discussed.

## 2. Description of model

This section formulates a mathematical description of a Franz diffusion cell experiment for one substance under infinite dose conditions. In particular, it introduces notation used in the remainder of the work. At first, a description of the model geometry is given. The next subsection formulates the distribution of the substance, or more precisely its concentration, in terms of a partial differential equation. How this model is related to physical quantities measured in the experiment is derived afterwards. The section concludes with a brief description of the numerical methods which were applied in the solution process.

### 2.1. Model geometry

The model used in this article is based on the two-dimensional *brick-and-mortar model* which was used for the SC in [31]. A full-thickness or *extended skin model* is derived from this model by adding a homogeneous compartment of constant size for the deeper skin layers (DSL). It is the role of this compartment to guarantee proper outflow conditions at the interface between SC and epidermis. It does not focus on a precise resolution of the processes in epidermis and dermis. This simplification is admissible as far as only a structural resolution of the SC and the barrier property of full thickness skin are concerned. The resulting geometry of the extended skin model is depicted in Fig. 1.

Formally, the domain consists of three different phases $\Omega_{\mathrm{cor}}$, $\Omega_{\mathrm{lip}}$, and $\Omega_{\mathrm{DSL}}$, representing either the corneocytes, the surrounding lipid matrix or the DSL. The corneocytes are fully staggered in $n = 16$ layers. The remaining geometric parameters are the diameter of lipid channel $\delta = 0.1$ μm, the corneocyte height $h_{\mathrm{cor}} = 1$ μm, the corneocyte width $L_{\mathrm{cor}} = 30$ μm, and the height of the DSL compartment $h_{\mathrm{DSL}} = 1.5$ mm. These parameters are summarised in Table 1.

The neighbouring phases are separated by two interfaces $\Gamma_{\mathrm{cor,lip}}$ and $\Gamma_{\mathrm{DSL,lip}}$, respectively. The corneocytes and the deeper skin layers do not share a common interface. The domain is confined by boundaries $\Gamma_{\mathrm{in}}$, $\Gamma_{\mathrm{out}}$ and $\Gamma_{\mathrm{side}}$. For the remainder of this work an index set $I = \{\mathrm{cor}, \mathrm{lip}, \mathrm{DSL}\}$ will be used in order to avoid an unnecessarily abundant notation. Subdomains and interfaces are then, for instance, referred to by the symbols $\Omega_i$ and $\Gamma_{i,j}$ for $i \neq j$ and $i,j \in I$ (Table 2).

### 2.2. Model equations

It is assumed that transport in each phase is due to Fick's second law of diffusion,

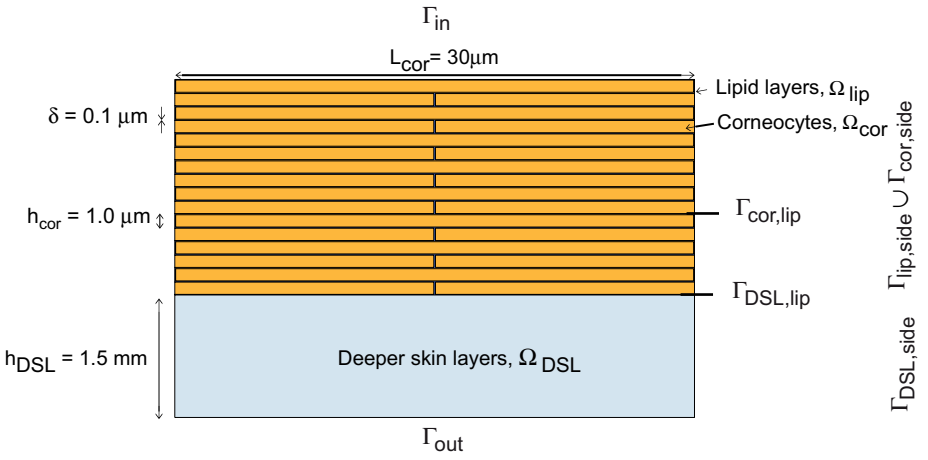


Fig. 1. The extended brick-and-mortar model for human stratum corneum and viable epidermis and dermis. Diffusion occurs through lipid layers, corneocytes and deeper skin layers (DSL). Interfaces, domains and parameters are given in Table 2.

Table 1
Description of the model geometry

| | |
|---|---|
| $\delta$ | Lipid layer thickness |
| $L_{\mathrm{cor}}$ | Corneocyte length |
| $h_{\mathrm{cor}}$ | Corneocyte height |
| $h_{\mathrm{DSL}}$ | Height of DSL compartment |
| $\mathscr{L}_k$ | $k$th SC layer |
| $d_k$ | Average depth of $\mathscr{L}_k$; distance of the centre mass of $\mathscr{L}_k$ to the top surface $\Gamma_{\mathrm{in}}$ |

Table 2
Domains and interfaces of the model membrane

| Domains and interfaces | Symbol | Diffusion coefficient | Partition coefficient | Concentration |
|---|---|---|---|---|
| (Donor compartment) | | n.a. | | $c_{\mathrm{don}}$ |
| Interface | $\Gamma_{\mathrm{in}}$ | | $K_{\mathrm{lip/don}}$ | |
| Lipid layers | $\Omega_{\mathrm{lip}}$ | $D_{\mathrm{lip}}$ | | $c_{\mathrm{lip}}$ |
| Interface | $\Gamma_{\mathrm{cor/lip}}$ | | $K_{\mathrm{cor/lip}}$ | |
| Corneocytes | $\Omega_{\mathrm{cor}}$ | $D_{\mathrm{cor}}$ | | $c_{\mathrm{cor}}$ |
| ⋮ | | | | |
| Lipid layers | $\Omega_{\mathrm{lip}}$ | $D_{\mathrm{lip}}$ | | $c_{\mathrm{lip}}$ |
| Interface | $\Gamma_{\mathrm{DSL/lip}}$ | | $K_{\mathrm{DSL/lip}}$ | |
| Deeper skin layers | $\Omega_{\mathrm{DSL}}$ | $D_{\mathrm{DSL}}$ | | $c_{\mathrm{DSL}}$ |
| Interface | $\Gamma_{\mathrm{out}}$ | | $K_{\mathrm{DSL/acc}}$ | |
| (Receptor compartment) | | n.a. | | $c_{\mathrm{acc}}$ |

$$\partial_t c_i(x,t) - \mathrm{div}(D_i \nabla c_i(x,t)) = 0 \tag{1}$$

for $t>0$, $x\in\Omega_i$, $i\in I$. On the interfaces between the phases two different types of transmission conditions apply. Partitioning between the different phases is modelled using a partition coefficient $K_{i/j}$,

$$c_i(x,t) = K_{i/j} c_j(x,t) \tag{2}$$

for $t>0$, $x\in\Gamma_{i,j}$, $i\neq j$. As for several hydrophilic and also some lipophilic compounds their intra-corneocyte presence has been visualised, $K_{\mathrm{cor/lip}}\neq 0$ needs to be considered at the lipid–corneocyte interface [37–40]. Additionally, the flux across an interface must be continuous due to mass conservation, which means that

$$\left(D_i \nabla c_i(x,t) + D_j \nabla c_j(x,t)\right)\cdot n(x) = 0 \tag{3}$$

holds for $t>0$, $x\in\Gamma_{i,j}$, $i\neq j$ and any normal $n$ to $\Gamma_{i,j}$. The initial values used are given by

$$c_i(x,0) = 0, \tag{4}$$

for $x\in\Omega_i$, $i\in I$. The boundary conditions are given by

$$c_{\mathrm{lip}}(x,t) = c_{\mathrm{lip}}^{(\mathrm{in})}, x\in\Gamma_{\mathrm{in}}, \tag{5}$$

$$c_{\mathrm{DSL}}(x,t) = c_{\mathrm{DSL}}^{(\mathrm{out})}, x\in\Gamma_{\mathrm{out}}, \tag{6}$$

$$\frac{\partial c_i}{\partial n}(x,t) = 0,\ x\in\Gamma_{i,\mathrm{side}},\ i\in\{\mathrm{lip},\ \mathrm{cor}\} \tag{7}$$

and $$\frac{\partial c_{\mathrm{DSL}}}{\partial n}(x,t) = 0, x\in\Gamma_{\mathrm{DSL,side}}, \tag{8}$$

for $t>0$. The concentrations on the outer boundaries are usually induced by concentrations in the donor and the acceptor compartments, $c_{\mathrm{don}}$ and $c_{\mathrm{acc}}$. In this model they are assumed to be constant and have constant partition coefficients as well:

$$c_{\mathrm{lip}}^{(\mathrm{in})} = K_{\mathrm{lip/don}} c_{\mathrm{don}}, \tag{9}$$

$$c_{\mathrm{DSL}}^{(\mathrm{out})} = K_{\mathrm{DSL/acc}} c_{\mathrm{acc}}. \tag{10}$$

The original brick-and-mortar model is obtained by removing the subdomain $\Omega_{\mathrm{DSL}}$ and by an identification of the interfaces $\Gamma_{\mathrm{DSL,lip}}$ and $\Gamma_{\mathrm{out}}$. In this case, the condition in Eq. (8) becomes empty and Eqs. (6) and (10) must be substituted by

$$c_{\mathrm{lip}}(x,t) = c_{\mathrm{lip}}^{(\mathrm{out})}, x\in\Gamma_{\mathrm{out}}, \tag{11}$$

$$c_{\mathrm{lip}}^{(\mathrm{out})} = K_{\mathrm{lip/acc}} c_{\mathrm{acc}}. \tag{12}$$

Note that protein binding effects of the keratin-filled corneocytes, as reported, e.g., by [41], are not included in the model. This can be done, e.g., by adding a factor before the time derivative in Eq. (1) for $i=\mathrm{cor}$.

### 2.3. Aggregation of quantities

For each time $t > 0$ the amount of substance passing through an interface $\Gamma \subset \partial\Omega_{\text{lip}}$ is given by

$$j(\Gamma, t) = -\int_{\Gamma} (D_{\text{lip}} \nabla c_{\text{lip}}(x,t)) \cdot n \, \mathrm{d}\mu.$$

When $\Gamma$ is a part of $\partial\Omega$, $n$ should be chosen as an outward normal to obtain a proper direction of the flow. As it is often desirable to normalise this quantity with respect to an area of unit size, the flux is defined by

$$J(\Gamma, t) = \frac{j(\Gamma, t)}{A(\Gamma)}.$$

Here $A(\cdot)$ refers to the area operator. In Franz-cell diffusion experiments, membranes are often characterised by the steady-state flux $J_\infty = \lim_{t\to\infty} J(\Gamma_{in}, t)$. In the experiment, concentrations are always aggregated by inspecting pools of strips, each of them assigned to a certain depth of the SC. To compare the results, the same must be done in the simulation. For $k = 1, \ldots, 16$, we define the $k$th SC layer by

$$\mathscr{L}_k = \{x \in \Omega : (k-1)(h_{\text{cor}} + \delta) \leqslant \text{dist}(x, \Gamma_{in}) \leqslant k(h_{\text{cor}} + \delta)\}.$$

This definition involves the distance between $x \in \Omega$ and $\Gamma_{\text{in}}$, which is given by $\text{dist}(x, \Gamma_{\text{in}}) = \min_{y\in\Gamma_{\text{in}}} |x - y|$. The (average) depth of $\mathscr{L}_k$ within the SC is

$$d_k = \left(k - \frac{1}{2}\right)(h_{\text{cor}} + \delta)$$

which is the average distance between $\mathscr{L}_k$ and $\Gamma_{in}$. The average concentration $\bar{c}_k$ in $\mathscr{L}_k$ is defined by

$$\bar{c}_k = \frac{1}{\int_{\mathscr{L}_k} 1 \mathrm{d}x} \int_{\mathscr{L}_k} c(x) \mathrm{d}x, \tag{13}$$

where $c(x) \equiv c_i(x)$ for $x \in \Omega_i$, $i \in \{\text{cor}, \text{lip}\}$. Plotting the pairs $(d_k, \bar{c}_k)$ for $k = 1, \ldots, 16$ results in discrete concentration–depth-profiles.

### 2.4. Numerical techniques

Before computations can be performed, the system has to be transformed to a dimensionless form. This is a trivial task, but it is stated formally in Section A.1 for the sake of completeness. The dimensionless partial differential equation is then solved numerically using the Rothe method: first the time is discretised using a fractional-step-$\theta$-scheme, cf. [42,43]. The resulting two-dimensional problem is solved using a finite-volume-scheme [44,45]. The whole process leads to large linear systems of equations which are solved using an algebraic-multigrid method [46,47]. By transforming the variable back into the original dimensions, the desired quantities can be computed.

## 3. Model and experiment

This section gives a summary of facts to be kept in mind, when comparing experiment and simulation. Input parameters for the simulation were determined in the companion study [1] for a Franz diffusion cell with an aqueous donor and an aqueous receptor compartment. The substances considered therein are flufenamic acid (FFA) and caffeine. Though the model discussed so far neither includes a donor nor an acceptor compartment, Eqs. (9) and (10) already describe a Franz diffusion cell with infinite dose conditions. For reasons of simplification, perfect sink conditions will be assumed in the deeper skin regions, i.e., $c_{\text{DSL}}^{(\text{out})} = c_{\text{acc}} = 0$, for the remainder of this work.

### 3.1. Input parameters

The computational model relies on seven input parameters. The membrane is characterised by the diffusion coefficients $D_{\text{lip}}$, $D_{\text{cor}}$ and $D_{\text{DSL}}$ and the partition coefficients $K_{\text{cor/lip}}$ and $K_{\text{DSL/lip}}$. An additional partition coefficient $K_{\text{lip/don}}$ and a constant concentration $c_{\text{don}}$ describe the donor compartment, cf. Eq. (9).

Hansen et al. describe in [1], how $D_{\text{DSL}}$, $D_{\text{lip}}$, and $K_{\text{lip/don}}$ can directly be determined in an experiment. The quantity $c_{\text{don}}$ is a free input parameter. In the case of the tape stripping experiment it is given by the concentration used in the donor compartment. The remaining three parameters $D_{\text{cor}}$, $K_{\text{cor/lip}}$, and $K_{\text{DSL/lip}}$ are hidden from direct access due to the heterogeneous structure and the small length scales of the SC membrane. In general, only average concentrations are available for the SC. Using a definition in analogy to Eq. (13), this yields an apparent partition coefficient $K_{\text{SC/don}}$ between donor and the first layer of the SC membrane. Nevertheless, this yields access to the partition coefficients $K_{\text{cor/lip}}$ and $K_{\text{DSL/lip}}$ by using the relative volume fractions of lipids and corneocytes in the SC.

A similar approach must be taken to determine the diffusion coefficient in the corneocytes. While $D_{\text{lip}}$ and $D_{\text{DSL}}$ are determined, e.g., by flux experiments, this does not carry over to $D_{\text{cor}}$. Yet this quantity can be derived from steady-state flux through the SC membrane. Until the end of the following subsection, the model is restricted to an SC-only geometry. On this membrane it is possible to define an apparent diffusion coefficient $D_{\text{SC}}$: for a homogeneous medium $D_{\text{SC}} = D_{\text{lip}} = D_{\text{cor}}$ and $K_{\text{cor/lip}} = 1$ hold, and the steady-state flux is given by Fick's first law of diffusion:

$$J_\infty^{(\text{hom})} = \left(-D_{\text{lip}} \nabla c_{\text{lip}}\right) \cdot n = -D_{\text{lip}} \frac{c_{\text{lip}}^{(\text{out})} - c_{\text{lip}}^{(\text{in})}}{h_{\text{SC}}}. \tag{14}$$

For a heterogeneous membrane the apparent diffusion coefficient $D_{\text{SC}}$ can be defined analogously, of course. It is implicitly given by the steady-state flux:

$$J_\infty = -D_{\text{SC}} \frac{c_{\text{lip}}^{(\text{out})} - c_{\text{lip}}^{(\text{in})}}{h_{\text{SC}}}. \tag{15}$$

Solving for $D_{\text{SC}}$ finally yields

$$D_{\text{SC}} = \frac{J_\infty \cdot h_{\text{SC}}}{c_{\text{lip}}^{(\text{in})} - c_{\text{lip}}^{(\text{out})}}, \tag{16}$$

where the right hand side of this equation is accessible in both simulation and experiment. An immediate consequence of Eqs. (14) and (15) is the identity

$$J_\infty = \frac{D_{SC}}{D_{lip}} J_\infty^{(hom)},$$

which explains the (artificial) definition of $D_{SC}$. The quotient $D_{SC}/D_{lip}$ is the constant indicating, how the flux through the heterogeneous SC membrane differs from a homogeneous membrane with the same thickness. This interpretation will be used in the subsequent subsection to derive a value for $D_{cor}$.

### 3.2. Corneocyte diffusion

It is shown in Section A.2 that for a fixed geometry the flux $J_\infty$ is described by a function which is linear in $D_{lip}$ and additionally depends on the variable

$$\xi = \frac{D_{cor}}{D_{lip}} K_{cor/lip} \tag{17}$$

only. By definition, cf. Eq. (16), the same must be true for the apparent diffusion coefficient. This behavior is mentioned earlier in the literature [19,26,33] using a variable $\sigma = 1/\xi$. A short and rigorous proof for this fact is given in Section A.2 of the Appendix A. The argumentation is valid for all models based on diffusion equations, and is in particular independent of geometric assumptions, e.g., the shape of the corneocytes.

The role of the dimensionless variable $\xi$ should be elucidated: It is defined by the product of the speed of diffusion within the corneocytes, which is evaluated relative to the lipids, and the partition coefficient between those two phases. When it comes to membrane permeability, both quantities can be traded into each other. Slow corneocyte diffusion can be compensated by an increase in the partitioning into the corneocytes and vice versa, little partitioning can be compensated by faster diffusion. In particular two limit cases are of interest. For $\xi \to 0$ an impermeable corneocyte membrane is obtained; there is neither a partitioning of substance into the corneocytes nor a diffusion within. Analogously $\xi \to \infty$ characterises a highly permeable corneocyte membrane; an infinite amount partitions into the corneocytes and shows an instantaneous diffusion behavior.

These two cases lead to the minimal and maximal apparent SC-diffusion coefficients which are denoted by $D_{SC,0}$ and $D_{SC,\infty}$, respectively. Both coefficients depend on the geometry. As diffusion in the homogeneous membrane is typically in between those cases, the constants should satisfy the inequality $D_{SC,0} < D_{lip} < D_{SC,\infty}$. For the brick-and-mortar geometries in this work the relation between $D_{SC}$ and $\xi$ is given in terms of the very efficient approximation

$$D_{SC}(\xi) \approx D_{SC,0} + \frac{D_{SC,\infty} - D_{SC,0}}{1 + \left(\frac{D_{SC,\infty} - D_{lip}}{D_{lip} - D_{SC,0}}\right) \Big/ \xi}. \tag{18}$$

The derivation is found in Section A.3 of the Appendix A. The right hand side characterises a function of $\xi$ of sigmoid shape on a logarithmic scale, with a range in the interval $[D_{SC,0}, D_{SC,\infty}]$. Solving Eq. (18) for a given $D_{SC}$ yields

$$\xi(D_{SC}) \approx \left(\frac{D_{SC,\infty} - D_{lip}}{D_{lip} - D_{SC,0}}\right) \Big/ \left(\frac{D_{SC,\infty} - D_{SC}}{D_{SC} - D_{SC,0}}\right). \tag{19}$$

Based on this approximation and Eq. (17), estimates for $D_{cor}$ are available given $D_{lip}$, $D_{SC}$ and $K_{cor/lip}$.

### 3.3. Concentration–depth-profiles

The simulation, as described by Eq. (13) in this work, and the experiment, as described in [1], allow to derive concentration–depth-profiles. Input data for both test compounds are derived from two different experimental setups which are discussed in the companion article in extenso. Both methods use the same techniques to determine $D_{lip}$, $D_{DSL}$, and $K_{lip/don}$. They differ in the way to determine $K_{SC/don}$, which affects $K_{cor/lip}$, $K_{DSL/lip}$, and $D_{cor}$. The first method, denoted by (M1), derives the partition coefficients from an equilibration experiment, in which concentrations are determined by measuring the loss of substance in the donor compartment. Alternatively, one can measure the substance extracted from the skin, yielding similar results. In a second method, denoted by (M2), the partition coefficient between donor and SC is obtained from a fit to the well-known solution of the one-dimensional heat equation, cf. [48]. The latter approach in particular also yields values for $D_{SC}$. As these turn out to be below the minimal membrane specific quantity $D_{SC,0}$, they were not considered in determining $D_{cor}$ according to Eq. (19).

## 4. Results

### 4.1. Apparent SC-diffusion coefficient

The illustration in Fig. 2 shows a plot of $D_{SC}/D_{lip}$ as a function of $\xi$ for the model membrane which is denoted by membrane A. The discrete data points are obtained from numerical simulation directly, while the continuous approximation corresponds to the right-hand side of Eq. (18). The geometry-dependent constants are $D_{SC,0}/D_{lip} = 0.0004675$ and $D_{SC,\infty}/D_{lip} = 11.0000000$.

To visualise the influence of changes in the geometry, membranes with different geometric parameters are considered as well. In a first step the lipid layer thickness of the model membrane is reduced by a factor of two, i.e., $\delta = 0.05$ μm (membrane B). In a second step, the relative cell overlap is gradually changed down to an overlap of zero. The minimal horizontal length of overlap of two neighbouring corneocyte blocks is $v = \frac{1}{2}(L_{cor} + \delta)$ (model

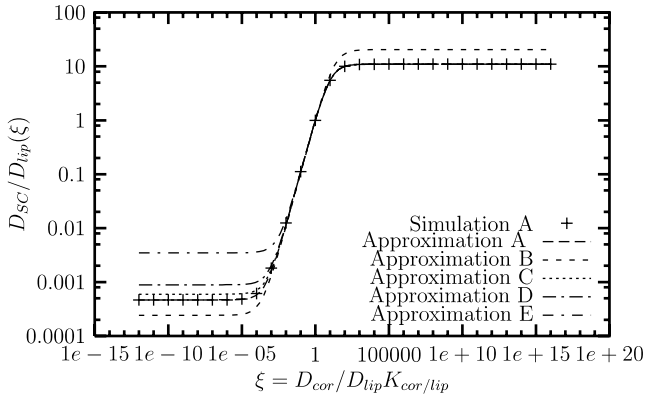


Fig. 2. The apparent diffusion coefficient $D_{SC}/D_{lip}$ for the model SC geometry is described as a function of $\xi = D_{cor}/D_{lip}K_{cor/lip}$. Simulated discrete data and corresponding approximation (model membrane, shown as membrane A, $\delta = 100$ nm, $v = \frac{1}{2}(L_{cor} + \delta)$). Additionally: approximation for membrane B using a thinner lipid layer ($\delta = 50$ nm, $v = \frac{1}{2}(L_{cor} + \delta)$) and approximations for membranes C–E with a decreased horizontal overlap ($\delta = 100$ nm and $v = \frac{1}{2}(L_{cor} + \delta), \frac{1}{4}(L_{cor} + \delta), \frac{1}{8}(L_{cor} + \delta)$, 0.0 μm. In all cases $L_{cor} = 30$ μm was used.).

membrane A, fully staggered), $v = \frac{1}{4}(L_{cor} + \delta)$ (membrane C), $v = \frac{1}{8}(L_{cor} + \delta)$ (membrane D) and $v = 0.0$ μm (membrane E, zero overlap), respectively. In all cases the continuous functions show an excellent agreement to the discrete data. Hence, the latter ones are omitted in the illustration for the sake of clarity.

### 4.2. Parameter studies

To visualise the influence of changes in the values of $D_{cor}/D_{lip}$ and $K_{cor/lip}$, parameter studies have been conducted. A representative test set of parameters consisted of values of

$$K_{cor/lip} \in \{0.01, 0.1, 1.0\}$$

and

$$\frac{D_{cor}}{D_{lip}} \in \{10^{-5}, 10^{-3}, 10^{-1}\}.$$

This results in nine concentration–SC-depth profiles which are shown in Fig. 3. Due to the influence on the concentration, they are grouped in three triples according to the $K_{cor/lip}$ value in ascending order. The remaining parameters in this study are given by $K_{lip/don}c_{don} = 1$ μg/ml, $K_{lip/DSL} = 1.0$, and $\frac{D_{DSL}}{D_{lip}} = 100.0$.

### 4.3. Concentration–depth-profiles

A summary of the input data is given in Table 3. The table is extended by two rows for the speed of diffusion in the corneocytes. The value $D_{cor}$ is determined according to Eq. (19). As this derivation is sensitive with respect to errors in the input data, an alternative estimate is introduced. This is denoted by $D^*_{cor}$ and its value is obtained from $D_{cor}$ by a reduction of one (caffeine) and two (FFA) orders of magnitude, respectively. This latter mentioned

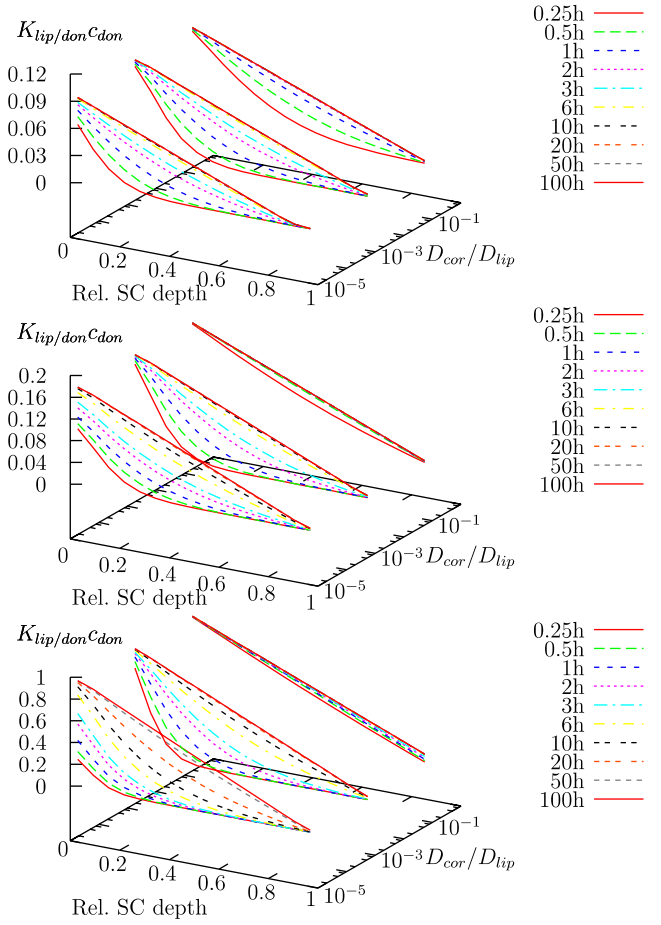


Fig. 3. Time dependence of concentration–SC-depth profiles for $K_{cor/lip} = 0.01$, 0.1, 1.0 (from top to bottom) and various values for $D_{cor}/D_{lip} = 10^{-1}, 10^{-3}, 10^{-5}$. Concentrations are shown relative to $K_{lip/don}$ $c_{don} = 1$ μg/ml. Parameters in DSL compartment: $K_{lip/DSL} = 1$, $D_{DSL}/D_{lip} = 100$. Times are normalised to $D_{lip} = 1.0$ μm$^2$/s $= 3.6 \times 10^{-5}$ cm$^2$/h.

Table 3
Experimental input parameters for simulation

| Parameter | Substance | | | |
|---|---|---|---|---|
| | Flufenamic acid | | Caffeine | |
| $D_{lip}$ (cm$^2$/h) | $1.1 \times 10^{-4}$ | | $2.1 \times 10^{-4}$ | |
| $D_{SC}$ (cm$^2$/h) | $1.7 \times 10^{-7}$ | | $1.4 \times 10^{-7}$ | |
| $D_{DSL}$ (cm$^2$/h) | $4.9 \times 10^{-3}$ | | $2.3 \times 10^{-3}$ | |
| $K_{lip/don}$ | 20.32 | | 2.15 | |
| $c_{don}$ (mg/ml) | 1.0 | | 12.5 | |
| | Experimental method | | | |
| | (M1) | (M2) | (M1) | (M2) |
| $K_{SC/don}$ | 16.20 | 5.88 | 4.51 | 4.70 |
| $K_{cor/lip}$ | 0.77 | 0.21 | 2.22 | 2.32 |
| $K_{DSL/lip}$ | 0.26 | 0.10 | 0.08 | 0.08 |
| $D_{cor}$ (cm$^2$/h) | $1.4 \times 10^{-7}$ | $5.1 \times 10^{-7}$ | $1.8 \times 10^{-8}$ | $1.7 \times 10^{-8}$ |
| $D^*_{cor}$ (cm$^2$/h) | $1.4 \times 10^{-9}$ | $5.1 \times 10^{-9}$ | $1.8 \times 10^{-9}$ | $1.7 \times 10^{-9}$ |

Mean values according to [1]. $D_{cor}$ and $D^*_{cor}$ determined according to Section 3.2.

quantity is used to generate the concentration–depth-profiles which are shown in Figs. 4–9. For each model substance results are plotted separately for incubation times

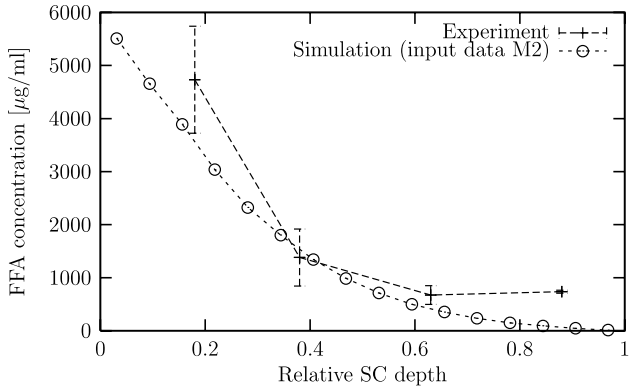


Fig. 4. Concentration–depth-profile for FFA at $t = 1$ h.

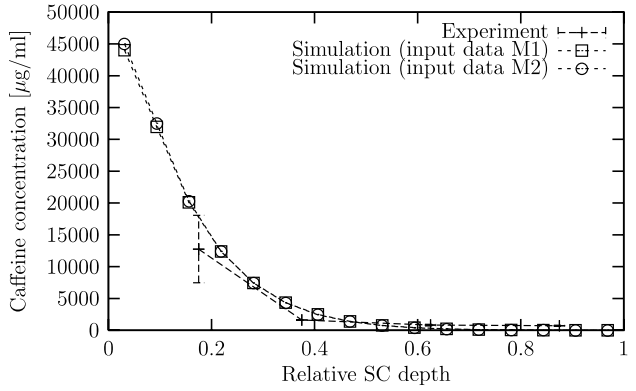


Fig. 5. Concentration–depth-profile for caffeine at $t = 1$ h.

of 1 h (Figs. 4 and 5), 2 h (Figs. 6 and 7) and 6 h (Figs. 8 and 9). As the input data for FFA contain a comparatively large value of $K_{SC/don}$ for (M1), an overestimation for $K_{cor/lip}$ is obtained. Hence, these results are excluded from the illustrations.

## 5. Discussion

While neglecting geometric information, the model presented in this work is based on first principles only. This is independent of the substance and yields excellent predictive qualities as long as the relevant parameters are determined accurately enough. Of course, this can be achieved mathematically by using parameter estimation and inverse modelling. However, this limits the predicitive power of the model, as it relies on an a-posteriori analysis. In order to avoid this, an experimental access to the relevant model coefficients is prefered in the study at hand.

The rationale for the choice of the test compounds is to show that the model is applicable independently of a substance's hydrophilic and lipophilic character, respectively. The main restriction is that the substances must show Fickian type diffusion behaviour. Therefore, a key assumption in this work is that both substances diffuse freely through the whole membrane. Note that although the

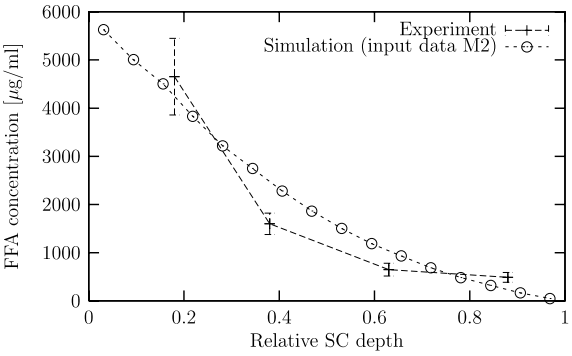


Fig. 6. Concentration–depth-profile for FFA at $t = 2$ h.

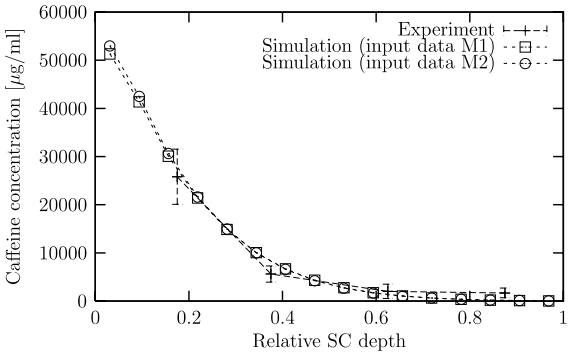


Fig. 7. Concentration–depth-profile for caffeine at $t = 2$ h.

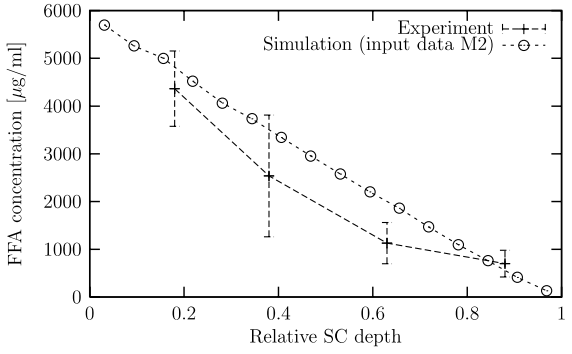


Fig. 8. Concentration–depth-profile for FFA at $t = 6$ h.

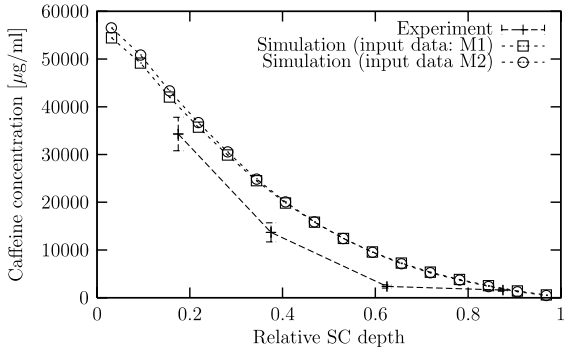


Fig. 9. Concentration–depth-profile for caffeine at $t = 6$ h.

molecular weight is not incorporated in the model directly, it naturally influences the diffusion properties. This may impair the applicability of the model for molecules with a particularly large molecular weight. Finally, keratin binding of flufenamic acid is not included in the model.

### 5.1. Apparent SC-diffusion coefficient

A comparison of membranes A and B in Fig. 2 yields that a change in the relative lipid layer thickness affects the scaling of the approximating function. A reduction of $\delta$ increases the maximal values for $D_{SC,\infty}/D_{lip}$ and decreases the minimal values for $D_{SC,0}/D_{lip}$. On the contrary, variations in the overlap of the corneocyte cells, as described by the graphs for membranes A, and C–E, affects the lower bound $D_{SC,0}/D_{lip}$ only. The latter observation explains, for instance, the differences in the barrier function between species (e.g., human vs. rat), between human skin and human skin equivalents as well as between normal and diseased skin.

For large values $\xi > 0.1$, the graphs for membranes A and C–E almost coincide. In the lower regimes, $\xi < 0.1$, especially membrane E, the case of overlap zero, is significantly different from the other cases. With respect to the data presented in Table 3, it must be mentioned that the experimental results are gathered in the lower regimes ($D_{SC}/D_{lip} = 1.5 \times 10^{-3}$ for FFA, and $D_{SC}/D_{lip} = 6.7 \times 10^{-4}$ for caffeine). This observation has two drawbacks: Firstly, the variation of geometric parameters in Section 4.1 shows that changes in the geometry affect the dependence of $D_{SC}/D_{lip}$ on $\xi$. The smaller the horizontal overlap is, the larger becomes the minimal effective membrane permeability. In this case, the resulting $\xi$ (and consequently also $D_{cor}$) is reduced. Secondly, the computation of $\xi$ is ill conditioned for $D_{SC} \to D_{SC,0}$. In Fig. 2 this is seen easily for small values of $\xi$, which correspond to almost identical values of $D_{SC}/D_{lip}$.

Despite these shortcomings it should be stressed that the concept and the results presented in Sections 3.2 and 4.1 extend to a multitude of membranes in cell biology and are applicable for all membranes of biphasic character.

### 5.2. Concentration–depth-profiles

The results for flufenamic acid are shown in Figs. 4, 6 and 8. The development of the profiles in time is similar for both simulation and experiment; the only exception is the linear profile for the simulation in Fig. 8. This is an indicator that steady state is reached after 6 h, which is not observed in the experiment. The quantitative precision is quite accurate, though not perfectly within the range of the experimental error. For caffeine, shown in Figs. 5, 7 and 9, the concentrations of the simulations show significantly better agreements with the experiment and are close to the range of experimental accuracy. Due to the similarity of input data for (M1) and (M2) for $K_{SC/don}$, the result of the simulations can hardly be distinguished.

Compared to the small incubation times of 1 and 2 h, experiment and simulation show comparatively large differences for an incubation time of 6 h. This is firstly caused by technical problems of the tape stripping technique. With increasing incubation times water enters into the SC and leads to a degradation of the structure. As a consequence, the spatial resolution of the tape stripping profiles is losing accuracy. Secondly, the mathematical model is lacking precision as it does not include swelling effects. As reported by Richter et al. [49], especially the thickness of the lowermost SC layers can be affected by water content. As such behavior is not included in the simulation, this may lead to an underestimation of the layer volume, and hence to an overestimation of the concentration. This is in particular true for the lowermost SC layers. Especially for flufenamic acid the results of simulation and experiment differ in this region. One reason can be the comparatively large depth of the DSL compartment. The smaller this compartment, the tighter is the coupling between the end of the membrane and the lowest SC layers.

Last it must be mentioned that one basic assumption of this work are equally sized and fully staggered SC layers. The effect of layers differing in their thicknesses will be subject to future research. The model also does not cover that the uppermost skin layer in the stratum corneum disiunctum is packed less tighten than in the lower SC layers.

### 5.3. Parameters

One input parameter of particular importance is the diffusion coefficient in the lipids: due to the introduced normalisation, all times in the simulation depend on $D_{lip}$. This is critical, as this is an apparent quantity itself. It is known, cf. [32], that lateral diffusion along the lipid bilayers is much faster than vertical diffusion through the lipid bilayers. Therefore, the experimental value for $D_{lip}$ must be regarded to be an averaged value already, which represents all micro scale effects of diffusion in the SC. This is implicitly taken into account in the analysis at hand. It is the major advantage of this approach that this average quantity is feasible experimentally, while it is uncertain, if diffusion is Fickian at all on much smaller scales.

The second important unknown is the diffusion coefficient $D_{cor}$. Although it is difficult to access this quantity experimentally, the method presented in Section 3.2 yields reasonable estimates. Yet, as visualised in Fig. 2, the method is sensitive against geometric information, such as the relative corneocyte overlap and the lipid layer thickness. The necessity to reduce $D_{cor}$ can be due to differences in the cell alignment. Although the cells are fully staggered in the model membrane used for the simulation, it is unlikely that this is exactly the case in natural geometries [50]. Instead, already a slight perturbance of the optimal overlap leads to an increase of $D_{SC,0}$ as can be seen in Fig. 2. For a constant observed value for $D_{SC}$, this corresponds to lower values for $D_{cor}$.

One of the first computer simulation studies to consider penetrant concentration–depth-profiles in the SC was the one from Watkinson et al. [51]. These authors modelled concentration–distance-profiles for the case of heterogeneous SC, however their analysis is only applicable to the steady-state transport. They argued that the diffusion coefficient decreases from outer to inner layers of the SC. Using variable diffusion and partition coefficient models Anissimov and Roberts [52] showed in a previous study that partition coefficient heterogeneity had a more profound effect on predicted fluxes than diffusion coefficient heterogeneity. In a further paper, cf. [53], they argued that the clobetasol propionate tape stripping data were most consistent with the partition coefficient decreasing exponentially for half the SC and then becoming a constant for the remaining SC. The analysis at hand shows, how diffusion in the corneocytes and partitioning are interrelated and can be compensated by one another. Although constant coefficients were used, good agreements of simulation and experiment are obtained.

The different values of $K_{\mathrm{SC/don}}$ and thus $K_{\mathrm{cor/lip}}$ for (M1) and (M2) for FFA in Table 3 require further investigations. One reason may be effects of protein binding, which is caused by compounds attaching to keratin fragments inside the corneocytes. This behavior is not included in the model. However, it is known, e.g., from [54], that in the steady state this is equivalent to a reduction of $D_{\mathrm{cor}}$. This is the reason, why the correction of $D_{\mathrm{cor}}$ was chosen to be stronger for FFA than for caffeine.

The time-dependent interplay between $D_{\mathrm{cor}}$ and $K_{\mathrm{cor/lip}}$ is visualised in Fig. 3. It can be observed that the larger the value of $K_{\mathrm{cor/lip}}$, the more extreme the reaction to changes in $D_{\mathrm{cor}}/D_{\mathrm{lip}}$. This is what must be expected: with increasing $K_{\mathrm{cor/lip}}$, the corneocytes become more and more important for the storage capacity of the SC. When the diffusion in the corneocytes is slow, the reservoirs fill up slowly. With respect to the SC-depth the influence on the uppermost layers is the strongest in this case.

## 6. Conclusion

This study presented an in-silico simulation of drug diffusion in an in-vitro diffusion experiment under infinite dose conditions. It is based on experimental input data as determined by Hansen et al. [1]. The substances considered in this work are flufenamic acid and caffeine, which serve as representatives for lipophilic and hydrophilic compounds, respectively.

By a comparison of experiment and simulation it was shown, which parameters are critical when performing simulations. The analysis of the underlying model leads to improved insights how the steady-state flux through the SC membrane on the one hand and the interaction of diffusion in and partitioning between lipid and corneocyte on the other hand are coupled. It is shown, how a corrected interpretation of the input parameters leads to very good agreements of the concentration–depth-profiles of experiment and simulation.

The future work will include enlarging the set of substances as well as studying the effect of protein binding on the permeability properties of the human skin. Additionally, it must be shown whether the achieved tools are also valid in three-dimensional models.

## Acknowledgements

Financial support of parts of this work by the Centre for Documentation and Evaluation of Alternatives to Animal Experiments at the Federal Institute for Risk Assessment, Berlin, is gratefully acknowledged. S. Hansen and D. Neumann were financially supported by the Deutsche Forschungsgemeinschaft (DFG Grant BIZ 4/1). The authors thank E.M. Ortinau for her assistance in preparing this manuscript.

## Appendix A

For the sake of a better understanding, the following passage tries to give a brief overview over the numerical and mathematical methods. For a vector field $\mathbf{F} : \Omega \subset \mathbb{R}^2 \to \mathbb{R}^2$ in two-dimensional space with components $\mathbf{F} = (F_1, F_2)$, the divergence is given by

$$\operatorname{div} \mathbf{F}(x) = \frac{\partial F_1(x)}{\partial x_1} + \frac{\partial F_2(x)}{\partial x_2}.$$

This corresponds to the limit case of the surface integral which is normalised by the volume for infinitely small volumes. Regarding the derivation of the formulas of the diffusion equations of the form

$$-\operatorname{div}(\alpha \nabla u) = f \text{ in } \Omega \tag{A.1}$$

the reader may want to refer to standard literature from physics, cf. [55]. A comprehensible mathematical overview on this topic, which also considers the effect of the transmission conditions, can be found, e.g., in [56].

### A.1. Dimensionless form

By dividing the concentrations $c_i$ by a density $\rho$, we obtain a dimensionless variable $u_i = c_i/\rho$. At the same time a characteristic length scale $\lambda$ and a characteristic time scale $\tau$ are introduced. The diffusion coefficients can then be written as

$$D_i = \alpha_i \frac{\lambda^2}{\tau} \tag{A.2}$$

with a dimensionless scalar value $\alpha_i > 0$. For the time being it is assumed that $\lambda = 1$ μm. The characteristic time scale $\tau$ is chosen, such that $\alpha_{\mathrm{lip}} = 1$ and consequently

$$D_i = D_{\mathrm{lip}} \alpha_i. \tag{A.3}$$

for $i \in \{\mathrm{lip,cor,DSL,SC}\}$. The variables are then coupled by

$$c_i(x,t) = \rho u_i(y,s)$$

where

$$t = s \cdot \tau \text{ and } x_k = y_k \cdot \lambda \tag{A.4}$$

for each component $k$ of the vector. As it becomes obvious in Eq. (A.4) all domains and interfaces also undergo a transformation. Therefore, $\Omega_i, \Gamma_{i,j}$ are substituted by their dimensionless counterparts $\widehat{\Omega}_i, \widehat{\Gamma}_{i,j}$. The dimensionless form of Eq. (1) is then, for instance, given by

$$\partial_s u_i - \operatorname{div}_y\left(\alpha_i \nabla_y u_i\right) = 0$$

for $s > 0$, $y \in \widehat{\Omega}_i$, and $i \in I$. Analogous results hold for the other equations, as can be verified in a straightforward manner. The equations of the dimensionless formulation are formally identical, but the diffusion coefficients $\alpha_i$, $i \in I$ are given relative to $D_{\text{lip}}$. As an obvious implication, the time scale is inversely proportional to $D_{\text{lip}}$, e.g., a reduplication of all diffusion coefficients is equivalent to accelerating the time scale by a factor of two. Yet, due to Eq. (A.3) a transformation to physical quantities remains easy, see Section A.2 for further examples. A list of the parameters used in the dimensionless formulation is found in Table A.1.

### A.2. Flux as a function

Within this subsection the computational domain is restricted to the SC again. The flux and the permeability for this membrane are functions of $\alpha_{\text{cor}}$ and $K_{\text{cor/lip}}$. Within the model both variables are positive constants, $\alpha_{\text{cor}}$, $K_{\text{cor/lip}} > 0$. Using the transformation $u_{\text{cor}} = K_{\text{cor/lip}} \bar{u}_{\text{cor}}$ a substitution of $u_{\text{cor}}$ by $\bar{u}_{\text{cor}}$ results in

$$\begin{aligned} \partial_s u_{\text{lip}} - \operatorname{div}(\alpha_{\text{lip}} \nabla_y u_{\text{lip}}) &= 0 \text{ in } \widehat{\Omega}_{\text{lip}}, \\ K_{\text{cor/lip}}(\partial_s \bar{u}_{\text{cor}}) - \operatorname{div}(\xi \nabla_y \bar{u}_{\text{cor}}) &= 0 \text{ in } \widehat{\Omega}_{\text{lip}} \end{aligned}$$

and

$$\begin{aligned} (\alpha_{\text{lip}} \nabla_y u_{\text{lip}} + \xi \nabla_y \bar{u}_{\text{cor}}) \cdot n &= 0, \\ u_{\text{lip}} &= \bar{u}_{\text{cor}} \text{ on } \widehat{\Gamma}_{\text{cor,lip}} \end{aligned}$$

with $\xi = \alpha_{\text{cor}} K_{\text{cor/lip}}$. Note that the piecewise defined function

$$u(x) = \begin{cases} u_{\text{lip}}(x), & x \in \widehat{\Omega}_{\text{lip}} \\ \bar{u}_{\text{cor}}(x), & x \in \widehat{\Omega}_{\text{cor}} \end{cases}$$

Table A.1
Parameters of the dimensionless formulation

| | |
|---|---|
| $u_{\text{lip}}, u_{\text{cor}}, u_{\text{DSL}}$ | Dimensionless drug concentration in lipid, corneocytes and deeper skin layers |
| $\alpha_{\text{cor}}, \alpha_{\text{SC}}, \alpha_{\text{DSL}}$ | Dimensionless diffusion coefficients relative to $D_{\text{lip}}$, e.g., $\alpha_{\text{cor}} = D_{\text{cor}}/D_{\text{lip}}$ |
| $\widehat{\Omega}_{\text{lip}}$, $\widehat{\Omega}_{\text{cor}}$, $\widehat{\Omega}_{\text{DSL}}$ | Domains after transformation |
| $\widehat{\Gamma}_{\text{cor,lip}}$, $\widehat{\Gamma}_{\text{lip,DSL}}$ | Interior interfaces after transformation |
| $\widehat{\Gamma}_{\text{in}}$, $\widehat{\Gamma}_{\text{side}}$, $\widehat{\Gamma}_{\text{out}}$ | Exterior interfaces after transformation |
| $\lambda$, $\tau$ | Characteristic length and time scale |

is continuous. As the solution $u_{\text{lip}}$ in the lipid channel is not affected by this transformation, the flux

$$J_\infty = \frac{D_{\text{lip}}\rho}{A(\widehat{\Gamma}_{\text{out}})} \lim_{s\to\infty} \int_{\widehat{\Gamma}_{\text{out}}} \nabla_y u_{\text{lip}}(y,s) \cdot n \mathrm{d}\mu$$

is also an invariant of the transformation. Consequently all membranes with identical values of $\xi$ yield the same fluxes. By definition, this carries over to the permeability and the effective diffusion coefficient of the SC. The latter one is from now on denoted by $\alpha_{\text{SC}} = D_{\text{SC}}/D_{\text{lip}}$. It should be stressed that the whole argumentation is independent of the dimension and the shape of the geometry.

### A.3. Effective diffusivity

Plotting the discrete data of $\alpha_{\text{SC}}$ as a function of $\xi$ results in a graph of sigmoid shape which is bounded between $\alpha_{\text{SC},0}$ and $\alpha_{\text{SC},\infty}$, cf. Fig. 2 (Simulation A). If $\alpha_{\text{SC}}$ can be represented by a continuous function, this representation must be of the type

$$\alpha_{\text{SC}}(\xi) = \alpha_{\text{SC},0} + \frac{\alpha_{\text{SC},\infty} - \alpha_{\text{SC},0}}{1 + \exp\left(\phi(\xi)\right)}, \tag{A.5}$$

where $\phi : \mathbb{R} \to \mathbb{R}$ is continuous, and satisfies

$$\lim_{\xi\to 0} \phi(\xi) = \infty \text{ and } \lim_{\xi\to\infty} \phi(\xi) = -\infty.$$

One approach is to use an affine linear transformation of the form

$$\phi(\xi) = \frac{\beta - \ln \xi}{\gamma}$$

with $\beta, \gamma \in \mathbb{R}$ and $\gamma > 0$. A homogeneous membrane leads to the constraint $\alpha_{\text{SC}}(1) = 1$, which is equivalent to the identity

$$\gamma = \beta / \ln\left(\frac{\alpha_{\text{SC},\infty} - 1}{1 - \alpha_{\text{SC},0}}\right).$$

Inserting this into (A.5) yields

$$\alpha_{\text{SC}}(\xi) = \alpha_{\text{SC},0} + \frac{\alpha_{\text{SC},\infty} - \alpha_{\text{SC},0}}{1 + \left(\frac{\alpha_{\text{SC},\infty}-1}{1-\alpha_{\text{SC},0}}\right)^{\left(1 - \frac{\ln \xi}{\beta}\right)}}.$$

The positive constant $\beta$ depends on the geometry and characterises the inflection point of the graph. For the geometry considered in this work, a non-linear regression analysis yields that $\beta \approx \ln(\frac{\alpha_{\text{SC},\infty}-1}{1-\alpha_{\text{SC},0}})$ is a good approximation and consequently

$$\alpha_{\text{SC}}(\xi) \approx \alpha_{\text{SC},0} + \frac{\alpha_{\text{SC},\infty} - \alpha_{\text{SC},0}}{1 + \left(\frac{\alpha_{\text{SC},\infty}-1}{1-\alpha_{\text{SC},0}}\right)/\xi}.$$

The latter is equivalent to Eq. (18), since $\alpha_{\text{SC}} = D_{\text{SC}}/D_{\text{lip}}$ holds, due to Eq. (A.3).

## References

[1] S. Hansen, A. Henning, A. Naegel, M. Heisig, G. Wittum, D. Neumann, K.-H. Kostka, J. Zbytovska, C.M. Lehr, U.F. Schaefer,

In-silico model of skin penetration based on experimentally determined input parameters. Part I: Experimental determination of partition and diffusion coefficients, Eur. J. Pharm. Biopharm. 68 (2007) 352–367 .
[2] A.D. Jones, I. Dick, J. Cherrie, M. Cronin, J.V. de Sandt, D. Esdaile, S. Iyengar, W. ten Berge, S. Wilkinson, C. Roper, S. Semple, C. de Heer, F. Williams, CEFIC Workshop on methods to determine dermal permeation for human risk assessment, Tech. Rep. TM/04/07, Institute of Occupational Medicine, Research Park North, Riccarton, Edinburgh, EHf4 4AP, Scotland, UK (2004).
[3] F.M. Williams, EDETOX. Evaluations and predictions of dermal absorption of toxic chemicals, Int. Arch. Occup. Environ. Health 77 (2) (2004) 150–151.
[4] Commission of the European Communities, Commission Proposal for a Regulation of the European Parliament and of the Council concerning the Registration, Evaluation, Authorisation and Restrictions of Chemicals (REACH), Establishing a European Chemicals Agency and amending Directive 1999/45/EC on the classification, packaging and labelling of dangerous preparations and Regulation (EC) from 29 October 2003, Brussels, 29.10.2003, COM (2003) 644 final.
[5] R. Guy, J. Hadgraft, Transdermal drug delivery: a simplified pharmacokinetic approach, Int. J. Pharm. 24 (1985) 267–274.
[6] R. Guy, J. Hadgraft, H. Maibach, A pharmacokinetic model for percutaneous absorption, Int. J. Pharm. 11 (1982) 119–129.
[7] K.D. McCarley, A.L. Bunge, Physiologically relevant one-compartment pharmacokinetic models for skin. 1. Development of models, J. Pharm. Sci. 87 (4) (1998) 470–481.
[8] M.B. Reddy, K.D. McCarley, A.L. Bunge, Physiologically relevant one-compartment pharmacokinetic models for skin. 2. Comparison of models when combined with a systemic pharmacokinetic model, J. Pharm. Sci. 87 (4) (1998) 482–490.
[9] K.D. McCarley, A.L. Bunge, Physiologically relevant two-compartment pharmacokinetic models for skin, J. Pharm. Sci. 89 (9) (2000) 1212–1235.
[10] K.D. McCarley, A.L. Bunge, Pharmacokinetic models of dermal absorption, J. Pharm. Sci. 90 (11) (2001) 1699–1719.
[11] G. Gienger, A. Knoch, H.P. Merkle, Modeling and numerical computation of drug transport in laminates: model case evaluation of transdermal delivery system, J. Pharm. Sci. 75 (1) (1986) 9–15.
[12] M. Wolf, Mathematisch-physikalische Berechnungs- und Simulationsmod elle zur Beschreibung und Entwicklung therapeutischer Systeme, Habilitation thesis, University of Bonn (1993) (in German).
[13] M. Schmauder, Diffusion through the human skin – an unexpected application of a PDE-black-box-solver, ZAMM 75 (1995) 707–708.
[14] K. Sugibayashi, T. Hayashi, T. Hatanaka, M. Ogihara, Y. Morimoto, Analysis of simultaneous transport and metabolism of ethyl nicotinate in hairless rat skin, Pharm. Res. 13 (6) (1996) 855–860.
[15] K. Sugibayashi, T. Hayashi, Y. Morimoto, Simultaneous transport and metabolism of ethyl nicotinate in hairless rat skin after its topical application: the effect of enzyme distribution in skin, J. Control. Release 62 (1-2) (1999) 201–208.
[16] R. Manitz, W. Lucht, K. Strehmel, R. Weiner, R. Neubert, On mathematical modeling of dermal and transdermal drug delivery, J. Pharm. Sci. 87 (7) (1998) 873–879.
[17] P. Boderke, K. Schittkowski, M. Wolf, H.P. Merkle, Modeling of diffusion and concurrent metabolism in cutaneous tissue, J. Theor. Biol. 204 (3) (2000) 393–407.
[18] K. Kubota, F. Dey, S. Matar, E. Twizell, A repeated-dose model of percutaneous drug absorption, Appl. Math. Model. 26 (2002) 529–544.
[19] G.C. Charalambopoulou, P. Karamertzanis, E.S. Kikkinides, A.K. Stubos, N.K. Kanellopoulos, A.T. Papaioannou, A study on structural and diffusion properties of porcine stratum corneum based on very small angle neutron scattering data, Pharm. Res. 17 (9) (2000) 1085–1091.
[20] H.F. Frasch, A random walk model of skin permeation, Risk Anal. 22 (2) (2002) 265–276.
[21] H.F. Frasch, A.M. Barbero, Steady-state flux and lag time in the stratum corneum lipid pathway: results from finite element models, J. Pharm. Sci. 92 (11) (2003) 2196–2207.
[22] A.M. Barbero, H.F. Frasch, Modeling of diffusion with partitioning in stratum corneum using a finite element model, Ann. Biomed. Eng. 33 (9) (2005) 1281–1292.
[23] K. George, K. Kubota, E.H. Twizell, A two-dimensional mathematical model of percutaneous drug absorption, Biomed. Eng. Online 3 (1) (2004) 18.
[24] K. George, A two-dimensional mathematical model of non-linear dual-sorption of percutaneous drug absorption, Biomed. Eng. Online 4 (2005) 40.
[25] T. Yotsuyanagi, W.I. Higuchi, A two phase series model for the transport of steroids across the fully hydrated stratum corneum, J. Pharm. Pharmacol. 24 (12) (1972) 934–941.
[26] A. Michaels, S. Chandrasekaran, J. Shaw, Drug permeation through human skin: theory and in vitro experimental measurement, AIChE 21 (5) (1975) 985–996.
[27] W.J. Albery, J. Hadgraft, Percutaneous absorption: theoretical description, J. Pharm. Pharmacol. 31 (3) (1979) 129–139.
[28] K. Tojo, Random brick model for drug transport across stratum corneum, J. Pharm. Sci. 76 (12) (1987) 889–891.
[29] R. Lange-Lieckfeldt, G. Lee, Use of a model lipid matrix to demonstrate the dependence of the stratum corneum's barrier properties on its internal geometry, J. Control. Release 20 (1992) 183–194.
[30] D.A. Edwards, R. Langer, A linear theory of transdermal transport phenomena, J. Pharm. Sci. 83 (9) (1994) 1315–1334.
[31] M. Heisig, R. Lieckfeldt, G. Wittum, G. Mazurkevich, G. Lee, Non steady-state descriptions of drug permeation through stratum corneum. I. The biphasic brick-and-mortar model, Pharm. Res. 13 (3) (1996) 421–426.
[32] M.E. Johnson, D. Blankschtein, R. Langer, Evaluation of solute permeation through the stratum corneum: lateral bilayer diffusion as the primary transport mechanism, J. Pharm. Sci. 86 (10) (1997) 1162–1172.
[33] T.-F. Wang, G.B. Kasting, J.M. Nitsche, A multiphase microscopic diffusion model for stratum corneum permeability. I. Formulation, solution, and illustrative results for representative compounds, J. Pharm. Sci. 95 (3) (2006) 620–648.
[34] A.M. Barbero, H.F. Frasch, Transcellular route of diffusion through stratum corneum: results from finite element models, J. Pharm. Sci. 95 (10) (2006) 2186–2194.
[35] B. Yu, C. Dong, P. So, D. Blankschtein, R. Langer, In vitro visualization and quantification of oleic acid induced changes in transdermal transport using two-photon fluorescence microscopy, J. Invest. Dermatol. 117 (1) (2001) 16–25.
[36] B. Yu, K.H. Kim, P.T.C. So, D. Blankschtein, R. Langer, Topographic heterogeneity in transdermal transport revealed by high-speed two-photon microscopy: determination of representative skin sample sizes, J. Invest. Dermatol. 118 (6) (2002) 1085–1088.
[37] B. Yu, K.H. Kim, P.T.C. So, D. Blankschtein, R. Langer, Visualization of oleic acid-induced transdermal diffusion pathways using two-photon fluorescence microscopy, J. Invest. Dermatol. 120 (3) (2003) 448–455.
[38] K.M. Hanson, M.J. Behne, N.P. Barry, T.M. Mauro, E. Gratton, R.M. Clegg, Two-photon fluorescence lifetime imaging of the skin stratum corneum pH gradient, Biophys. J. 83 (3) (2002) 1682–1690.
[39] U. Jacobi, T. Tassopoulos, C. Surber, J. Lademann, Cutaneous distribution and localization of dyes affected by vehicles all with different lipophilicity, Arch. Dermatol. Res. 297 (2006) 303–310.
[40] H.E. Bodde, I. van den Brink, H.K. Koerten, F.H.N. de Haan, Visualization of in vitro percutaneous penetration of mercuric chloride; transport through intercellular space versus cellular uptake through desmosomes, J. Control. Release 15 (1991) 227–236.
[41] K. Abdulmajed, C.M. Heard, C. McGuigan, W.J. Pugh, Topical delivery of retinyl ascorbate co-drug. 2. Comparative skin tissue and keratin binding studies, Skin Pharmacol. Physiol. 17 (6) (2004) 274–282.

[42] F. Harlow, E. Welch, Numerical calculation of time dependent viscous incompressible flow of fluid with free surface, Phys. Fluids 8 (1965) 2182–2189.
[43] A. Chorin, Numerical solution of the Navier-Stokes equations, Math. Comp. 22 (1968) 745–762.
[44] W. Hackbusch, On first and second order box schemes, Computing 41 (1989) 277–296.
[45] J. Bey, Finite-Volumen und Mehrgitter-Verfahren für elliptische Randwertprobleme, Advances in numerical mathematics, Teubner, 1998 (in German).
[46] C. Wagner, On the algebraic construction of multilevel transfer operators, Computing 65 (2000) 73–95.
[47] A. Naegel, Filternde algebraische Mehrgitterverfahren und Anwendungen, Master's thesis, University of Heidelberg (2005) (in German).
[48] F. Pirot, Y.N. Kalia, A.L. Stinchcomb, G. Keating, A. Bunge, R.H. Guy, Characterization of the permeability barrier of human skin in vivo, Proc. Natl. Acad. Sci. USA 94 (4) (1997) 1562–1567.
[49] T. Richter, C. Peuckert, M. Sattler, K. Koenig, I. Riemann, U. Hintze, K.-P. Wittern, R. Wiesendanger, R. Wepf, Dead but highly dynamic-the stratum corneum is divided into three hydration zones, Skin Pharmacol. Physiol. 17 (5) (2004) 246–257.
[50] P. Talreja, N.K. Kleene, W.L. Pickens, T.F. Wang, G.B. Kasting, Visualization of the lipid barrier and measurement of lipid pathlength in human stratum corneum, AAPS Pharm. Sci. 3 (2) (2001) E13.
[51] A. Watkinson, A. Bunge, J. Hadgraft, A. Naik, Computer simulation of penetrant concentration–depth profiles in the stratum corneum, Int. J. Pharm. 87 (1992) 175–182.
[52] Y.G. Anissimov, M.S. Roberts, Diffusion modeling of percutaneous absorption kinetics: 3. Variable diffusion and partition coefficients, consequences for stratum corneum depth profiles and desorption kinetics, J. Pharm. Sci. 93 (2) (2004) 470–487.
[53] B. Mueller, Y.G. Anissimov, M.S. Roberts, Unexpected clobetasol propionate profile in human stratum corneum after topical application in vitro, Pharm. Res. 20 (11) (2003) 1835–1837.
[54] W.R. Vieth, K.J. Sladek, A model for diffusion in a glassy polymer, J. Coll. Sci. 20 (1965) 1014–1033.
[55] E. Nelson, Dynamical Theories of Brownian Motion, 2nd ed., Princeton University Press, 2001.
[56] J. Crank, The Mathematics of Diffusion, Oxford University Press, London, 1975.